

Structure Transformation in $\text{Ca}_{1-x-\delta}\text{Sr}_\delta\text{La}_x\text{Ag}_{1-y}\text{Sb}$ ($0 \leq \delta \leq 0.7$) and Related Thermoelectric Properties

Jia Guo, Min Zhu, Xin Li, Xu-Tang Tao, and Sheng-Qing Xia*

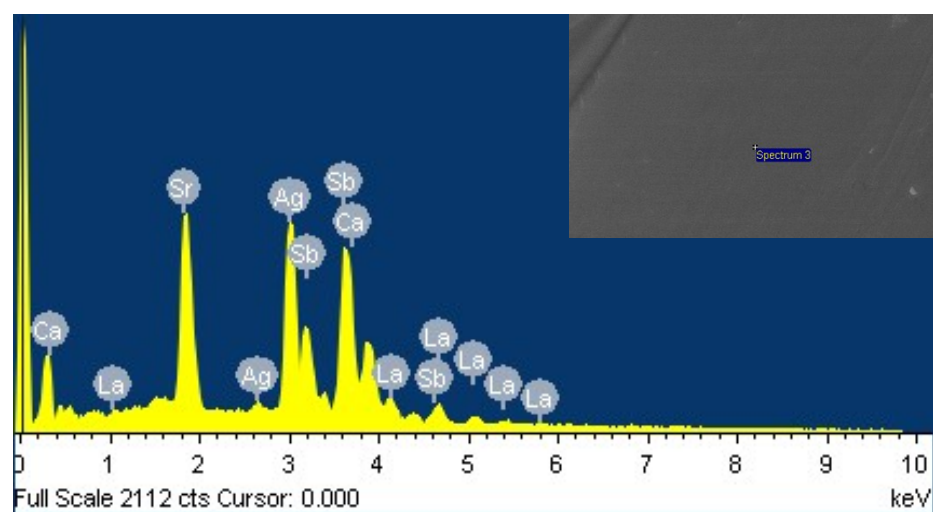
State Key Laboratory of Crystal Materials, Institute of Crystal Materials, Shandong University, Jinan, Shandong 250100, People's Republic of China

Supporting Information

Contents

1. EDS analyses on the compositions of single crystal of $\text{Ca}_{0.16(2)}\text{Sr}_{0.77(3)}\text{La}_{0.07(1)}\text{Ag}_{0.931(3)}\text{Sb}$.
2. **Table S1.** Selected crystal data and structure refinement parameters for $\text{Ca}_{0.16(2)}\text{Sr}_{0.77(3)}\text{La}_{0.07(1)}\text{Ag}_{0.931(3)}\text{Sb}$.
3. **Table S2.** Refined atomic coordinates and isotropic displacement parameters for $\text{Ca}_{0.16(2)}\text{Sr}_{0.77(3)}\text{La}_{0.07(1)}\text{Ag}_{0.931(3)}\text{Sb}$.
4. **Table S3.** Important interatomic distances (Å) in $\text{Ca}_{0.16(2)}\text{Sr}_{0.77(3)}\text{La}_{0.07(1)}\text{Ag}_{0.931(3)}\text{Sb}$.
5. **Table S4.** Unit cell parameters refined from the powder diffraction patterns of $\text{Ca}_{1-x-\delta}\text{Sr}_\delta\text{La}_x\text{Ag}_{0.89}\text{Sb}$ with various compositions.
6. **Figure S1.** Powder X-ray diffraction patterns for $\text{Ca}_{0.85}\text{La}_{0.15}\text{Ag}_{1-y}\text{Sb}$ ($y = 0.11, 0.13, 0.15$) materials.
7. **Figure S2.** Components of the electronic (a) and lattice thermal conductivity (b) for materials $\text{Ca}_{0.85}\text{La}_{0.15}\text{Ag}_{1-y}\text{Sb}$ ($y = 0.11, 0.13, 0.15$).
8. **Figure S3.** Powder X-ray diffraction patterns of material $\text{Ca}_{0.85}\text{La}_{0.15}\text{Ag}_{0.90}\text{Sb}$. The theoretical predictions of $\text{Ca}_{0.85}\text{La}_{0.15}\text{Ag}_{0.85}\text{Sb}$ and Ag were provided for comparison as well.
9. **Figure S4.** [AgSb] anionic framework structure of $\text{Ca}_{0.16(2)}\text{Sr}_{0.77(3)}\text{La}_{0.07(1)}\text{Ag}_{0.931(3)}\text{Sb}$ viewed along the b -axis. The long interlayered Ag-Sb distances (4.15 and 4.24 Å) as well as the almost planar [AgSb] net (in-plane Ag-Sb-Ag angle: 119.9°) both suggest high similarity to the SrAgSb structure, which evidently suggest the structure transformation of $\text{Ca}_{1-x-\delta}\text{Sr}_\delta\text{La}_x\text{Ag}_{1-y}\text{Sb}$ from the LiGaGe type towards the ZrBeSi type.
10. **Figure S5.** Temperature dependence of the heat capacity of materials $\text{Ca}_{1-\delta}\text{Sr}_\delta\text{La}_{0.15}\text{Ag}_{0.89}\text{Sb}$ ($\delta = 0.1, 0.2, 0.3, 0.4, 0.5, 0.6, 0.7$).
11. **Figure S6.** Band gaps (a) evaluated by the peaks of Seebeck coefficient measurements and corresponding effective mass (b) with various Sr contents.
12. **Figure S7.** Electronic band structures calculated for hypothetical LiGaGe-type $\text{Ca}_{1-x}\text{La}_x\text{Ag}_y\text{Sb}$ (left) and ZrBeSi-type SrAgSb (right).
13. **Figure S8.** Partial density of states (DOS) for ZrBeSi-type SrAgSb.

EDS analyses on the compositions of single crystal of $\text{Ca}_{0.16(1)}\text{Sr}_{0.76(1)}\text{La}_{0.07}\text{Ag}_{0.931(3)}\text{Sb}$.



| Element | Weight% | Atomic% | Composition |
|---------|---------|---------|-------------|
| Ca | 2.62 | 6.86 | 0.20 |
| Sr | 19.45 | 23.25 | 0.67 |
| Ag | 31.39 | 30.48 | 0.13 |
| Sb | 40.58 | 34.92 | 0.87 |
| La | 5.95 | 4.49 | 1 |

Table S1. Selected crystal data and structure refinement parameters for $\text{Ca}_{0.16(2)}\text{Sr}_{0.77(3)}\text{La}_{0.07(1)}\text{Ag}_{0.931(3)}\text{Sb}$.

| Formula | $\text{Ca}_{0.16(2)}\text{Sr}_{0.77(3)}\text{La}_{0.07(1)}\text{Ag}_{0.931(3)}\text{Sb}$ |
|--|--|
| fw/ $\text{g}\cdot\text{mol}^{-1}$ | 305.67 |
| T / K | 273(2) |
| Radiation, wavelength | Mo-K α , 0.71073 Å |
| Space group, No. | P6(3)mc (No.186) |
| Z | 2 |
| Cell dimensions | |
| a / Å | 4.7512(4) |
| c / Å | 8.3913(15) |
| V / Å ³ | 164.05(4) |
| $\rho_{\text{calc}} / \text{g}\cdot\text{cm}^{-3}$ | 6.188 |
| $\mu_{\text{Mo K}\alpha} / \text{cm}^{-1}$ | 2.693 |
| Final R indices ^a [$I > 2\sigma(I)$] | $R1 = 0.0132$ $wR2 = 0.0291$ |
| Final R indices ^a [all data] | $R1 = 0.0143$ $wR2 = 0.0297$ |

^a $R_1 = \sum ||F_o| - |F_c|| / \sum |F_o|$; $wR_2 = [\sum [w(F_o^2 - F_c^2)^2] / \sum [w(F_o^2)^2]]^{1/2}$, and $w = 1/[\sigma^2 F_o^2 + (A \cdot P)^2 + B \cdot P]$, $P = (F_o^2 + 2F_c^2)/3$; A and B are weight coefficients.

Table S2. Refined atomic coordinates and isotropic displacement parameters for $\text{Ca}_{0.16(2)}\text{Sr}_{0.77(3)}\text{La}_{0.07(1)}\text{Ag}_{0.931(3)}\text{Sb}$.

| Atoms | Wyckoff | occ. | x | y | z | U_{eq}^a (\AA^2) |
|-------|---------|-----------|-----|-----|-----------|--------------------------------------|
| Ag | 2b | 0.931(3) | 1/3 | 2/3 | 0.2465(5) | 0.0230(5) |
| Sb | 2b | 1 | 1/3 | 2/3 | 0.7519(4) | 0.0134(3) |
| La | 2a | 0.068(13) | 0 | 0 | 0 | 0.0145(3) |
| Sr | 2a | 0.77(3) | 0 | 0 | 0 | 0.0145(3) |
| Ca | 2a | 0.162(19) | 0 | 0 | 0 | 0.0145(3) |

^a U_{eq} is defined as one third of the trace of the orthogonalized U^{ij} tensor.

Table S3. Important interatomic distances (Å) in $\text{Ca}_{0.16(2)}\text{Sr}_{0.77(3)}\text{La}_{0.07(1)}\text{Ag}_{0.931(3)}\text{Sb}$.

| Atom pairs | | Distances (Å) |
|------------|---------------|---------------|
| Sr/La/Ca – | Sb \times 6 | 3.434(2) |
| | Ag \times 2 | 3.446(3) |
| | Ag \times 3 | 3.461(3) |
| Ag – | Sb \times 3 | 2.7435(3) |

Table S4. Unit cell parameters refined from the powder diffraction patterns of $\text{Ca}_{1-x}\text{Sr}_\delta\text{La}_x\text{Ag}_{0.89}\text{Sb}$ with various compositions.

| $\text{Ca}_{1-x}\text{Sr}_\delta\text{La}_x\text{Ag}_{0.89}\text{Sb}$ | a | b | c | $\alpha\beta\gamma$ |
|---|------------|----------|------------|---|
| x=0.15, $\delta=0$ | 4.703(1) Å | 4.703 Å | 7.792(2) Å | $\alpha=90^\circ$ $\beta=90^\circ$ $\gamma=120^\circ$ |
| x=0.15, $\delta=0.1$ | 4.706(1) Å | 4.706 Å | 7.853(1) Å | |
| x=0.15, $\delta=0.2$ | 4.708(1) Å | 4.708 Å | 7.935(1) Å | |
| x=0.15, $\delta=0.3$ | 4.720(1) Å | 4.720 Å | 7.985(3) Å | |
| x=0.15, $\delta=0.4$ | 4.730(2) Å | 4.730 Å | 8.070(4) Å | |
| x=0.15, $\delta=0.5$ | 4.729(1) Å | 4.729 Å | 8.136(3) Å | |
| x=0.15, $\delta=0.6$ | 4.742(1) Å | 4.742 Å | 8.217(1) Å | |
| x=0.15, $\delta=0.7$ | 4.749(2) Å | 4.749 Å | 8.299(7) Å | |
| x=0, $\delta=0.85$ | 4.762(1) Å | 4.762 Å | 8.532(1) Å | |

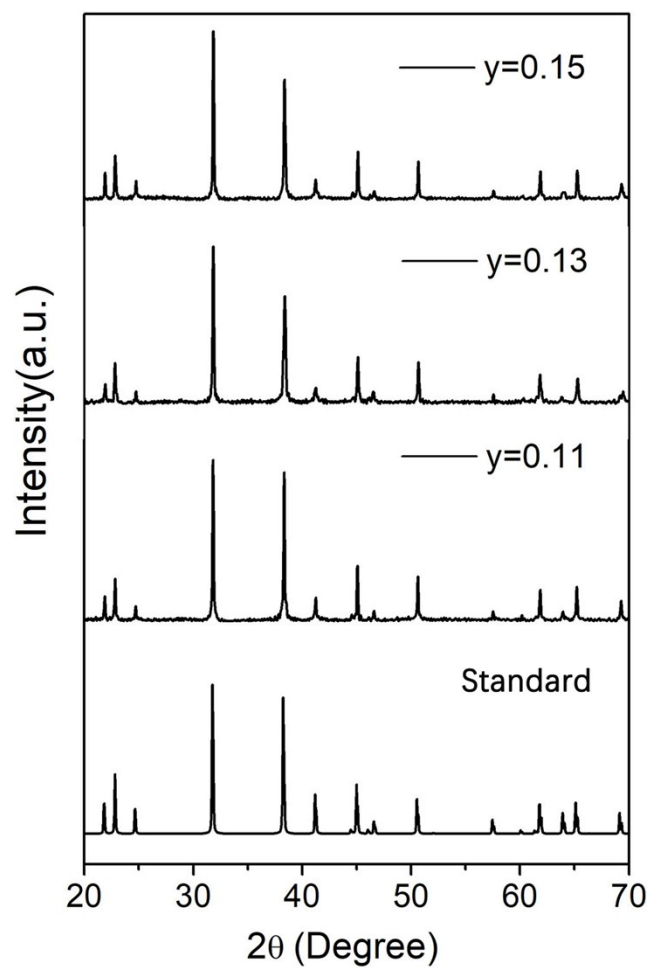


Figure S1. Powder X-ray diffraction patterns for $\text{Ca}_{0.85}\text{La}_{0.15}\text{Ag}_{1-y}\text{Sb}$ ($y = 0.11, 0.13, 0.15$) materials.

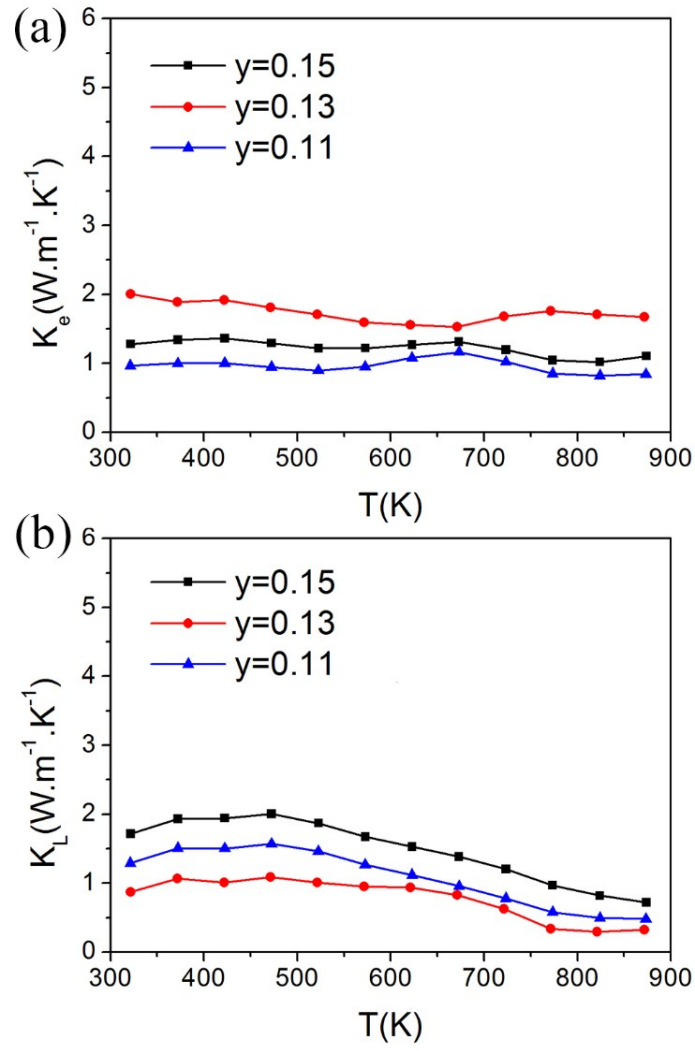


Figure S2. Components of the electronic (a) and lattice thermal conductivity (b) for materials $\text{Ca}_{0.85}\text{La}_{0.15}\text{Ag}_{1-y}\text{Sb}$ ($y = 0.11, 0.13, 0.15$).

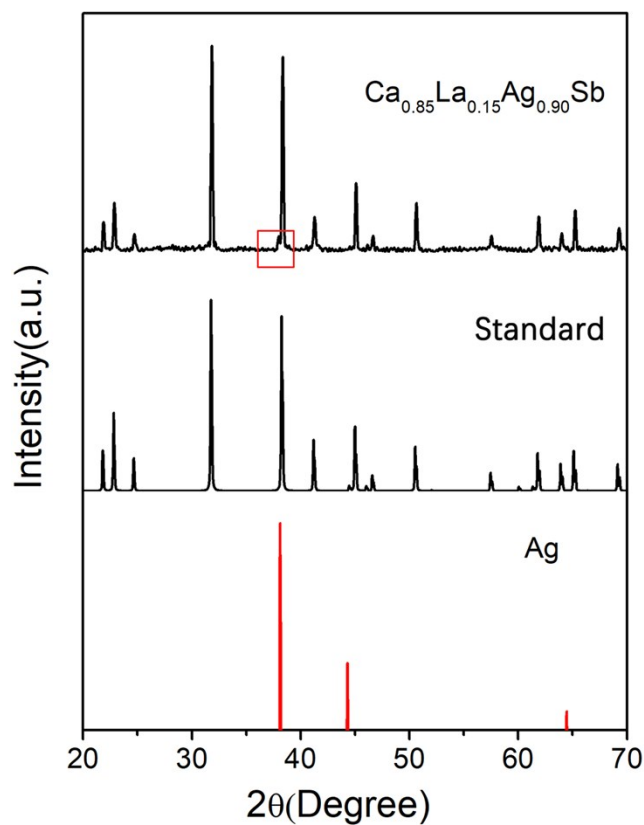


Figure S3. Powder X-ray diffraction patterns of material $\text{Ca}_{0.85}\text{La}_{0.15}\text{Ag}_{0.90}\text{Sb}$. The theoretical predictions of $\text{Ca}_{0.85}\text{La}_{0.15}\text{Ag}_{0.85}\text{Sb}$ and Ag were provided for comparison as well.

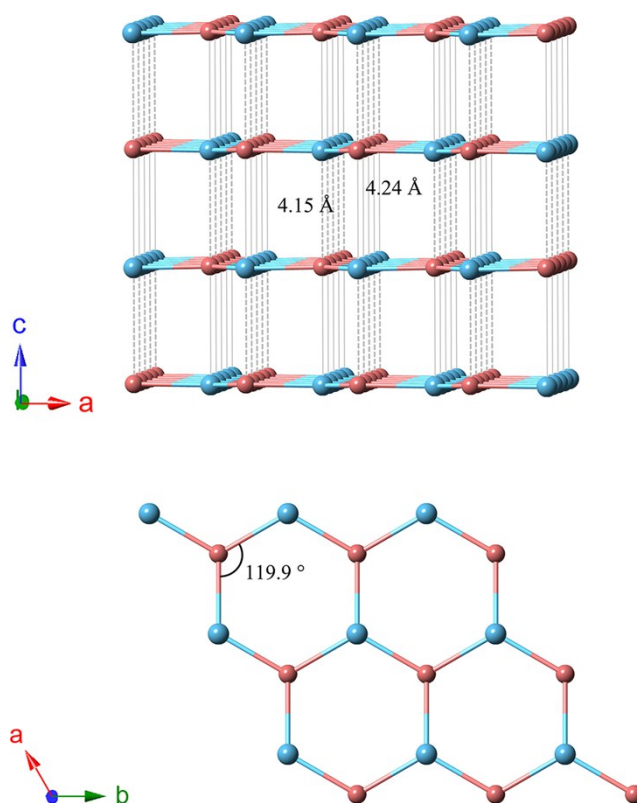


Figure S4. [AgSb] anionic framework structure of $\text{Ca}_{0.16(2)}\text{Sr}_{0.77(3)}\text{La}_{0.07(1)}\text{Ag}_{0.931(3)}\text{Sb}$ viewed along the b -axis. The long interlayered Ag-Sb distances (4.15 and 4.24 Å) as well as the almost planar [AgSb] net (in-plane Ag-Sb-Ag angle: 119.9°) both suggest high similarity to the SrAgSb structure, which evidently suggest the structure transformation of $\text{Ca}_{1-x-\delta}\text{Sr}_\delta\text{La}_x\text{Ag}_{1-y}\text{Sb}$ from the LiGaGe type towards the ZrBeSi type.

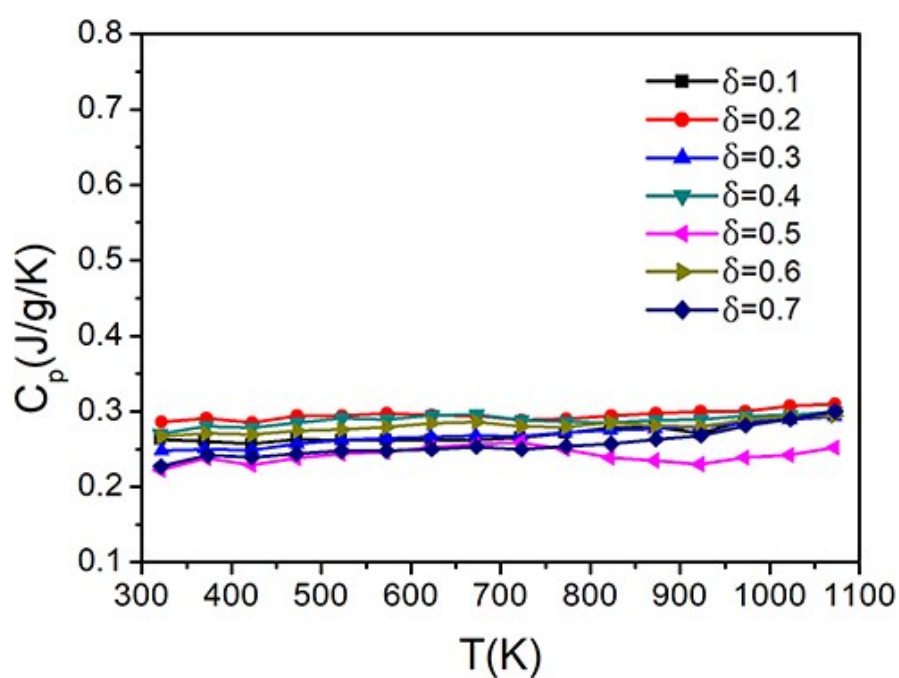


Figure S5. Temperature dependence of the heat capacity of materials $\text{Ca}_{1-\delta}\text{Sr}_\delta\text{La}_{0.15}\text{Ag}_{0.89}\text{Sb}$ ($\delta = 0.1, 0.2, 0.3, 0.4, 0.5, 0.6, 0.7$).

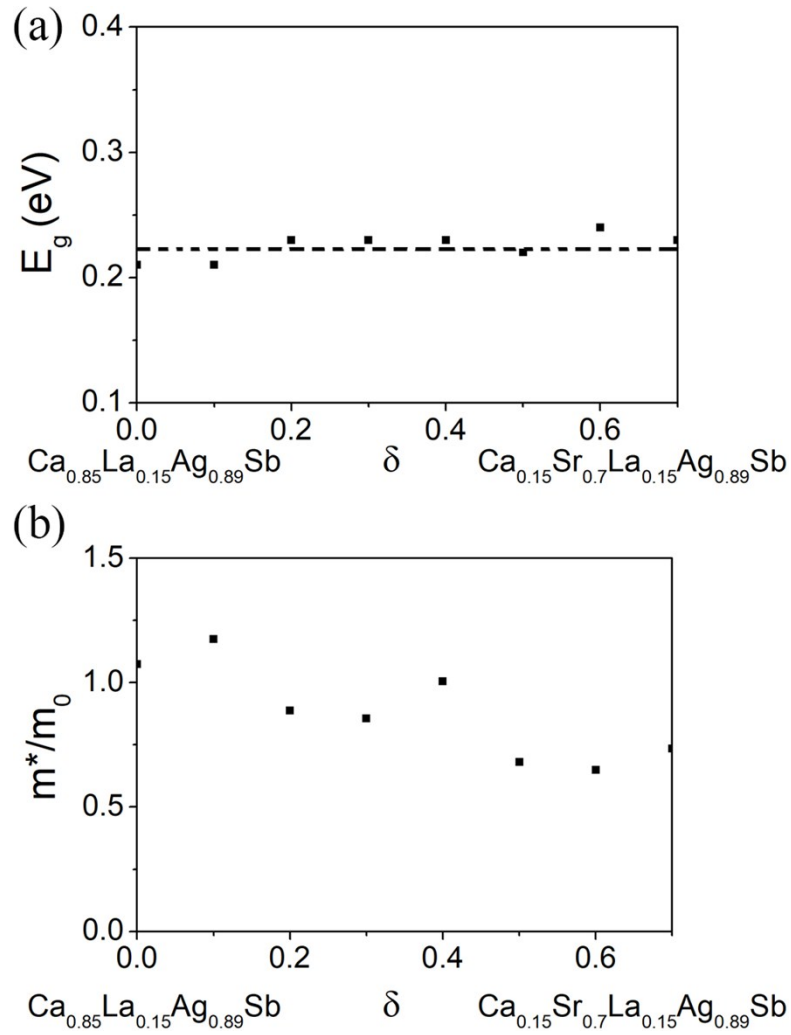


Figure S6. Band gaps (a) evaluated by the peaks of Seebeck coefficient measurements and corresponding effective mass (b) with various Sr contents in $\text{Ca}_{0.85-\delta}\text{Sr}_{\delta}\text{La}_{0.15}\text{Ag}_{0.89}\text{Sb}$.

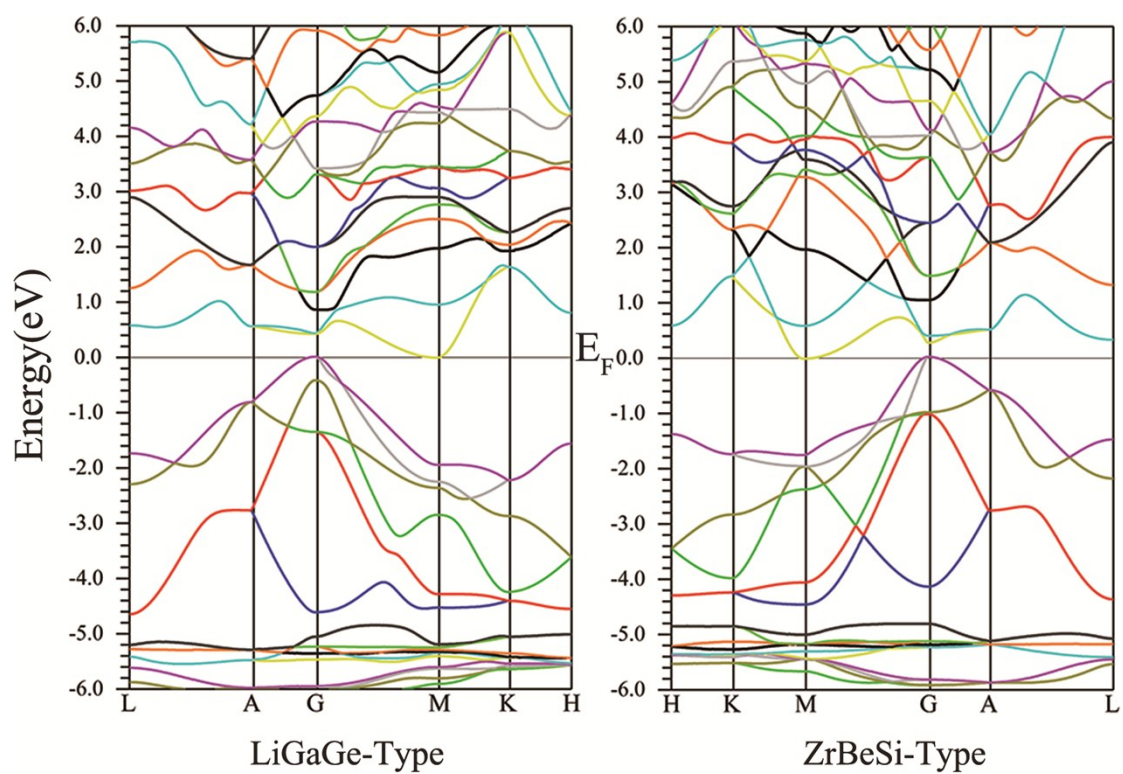


Figure S7. Electronic band structures calculated for hypothetical LiGaGe-type $\text{Ca}_{1-x}\text{La}_x\text{Ag}_y\text{Sb}$ (left) and ZrBeSi-type SrAgSb (right).

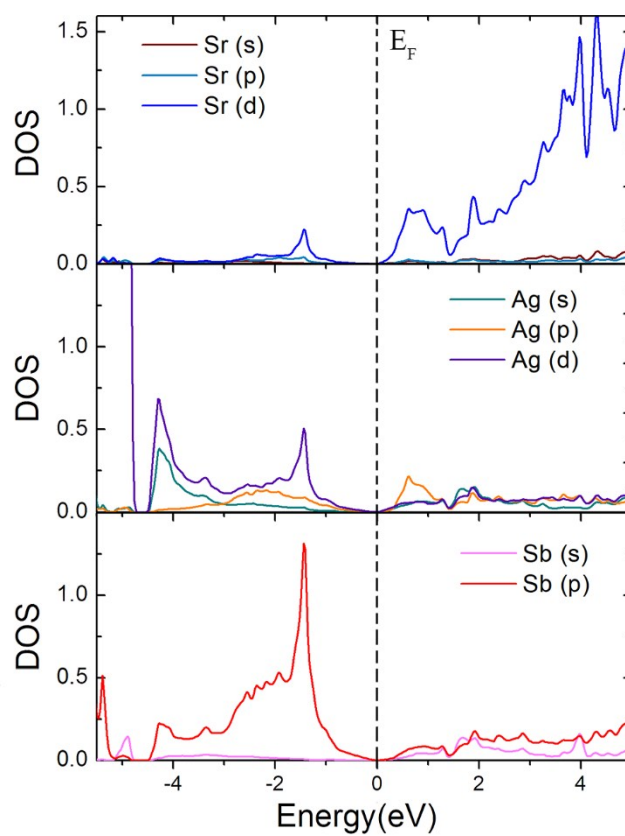


Figure S8. Partial density of states (DOS) for ZrBeSi-type SrAgSb.